Biochemistry

pubs.acs.org/biochemistry Article

Heat-Induced Conformational Transition Mechanism of Heat Shock Factor 1 Investigated by Tryptophan Probe

Soichiro Kawagoe, Munehiro Kumashiro, Takuya Mabuchi, Hiroyuki Kumeta, Koichiro Ishimori,* and Tomohide Saio*

Cite This: *Biochemistry* 2022, 61, 2897−2908 Read Online

ACCESS | Metrics & More | Article Recommendations | Supporting Information

ABSTRACT: A transcriptional regulatory system called heat shock response (HSR) has been developed in eukaryotic cells to maintain proteome homeostasis under various stresses. Heat shock factor-1 (Hsf1) plays a central role in HSR, mainly by upregulating molecular chaperones as a transcription factor. Hsf1 forms a complex with chaperones and exists as a monomer in the resting state under normal conditions. However, upon heat shock, Hsf1 is activated by oligomerization. Thus, oligomerization of Hsf1 is considered an important step in HSR. However, the lack of information about Hsf1 monomer structure in the resting state, as well as the structural change via oligomerization at heat response, impeded the understanding of the thermosensing mechanism through oligomerization. In this study, we applied solution biophysical methods, including fluorescence spectroscopy, nuclear magnetic resonance, and circular dichroism spectroscopy, to investigate the heat-induced conformational transition mechanism of Hsf1 leading to oligomerization. Our study showed that Hsf1 forms an inactive closed conformation mediated by intramolecular contact between leucine zippers (LZs), in which the intermolecular contact between the LZs for oligomerization is prevented. As the temperature increases, Hsf1 changes to an open conformation, where the intramolecular LZ interaction is dissolved so that the LZs can form intermolecular contacts to form oligomers in the active form. Furthermore, since the interaction sites with molecular chaperones and nuclear transporters are also expected to be exposed in the open conformation, the conformational change to the open state can lead to understanding the regulation of Hsf1-mediated stress response through interaction with multiple cellular components.

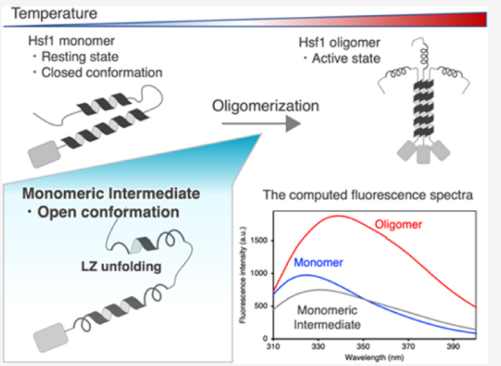

INTRODUCTION

Cells are exposed to a variety of stressful environments, including heat, reactive oxygen species, and pH changes throughout their lifetime.[1] To maintain proteome homeostasis under stress, organisms have a stress-responsive transcriptional regulatory system called heat shock response (HSR).[2−4] Heat shock factor-1 (Hsf1) plays a central role in the HSR system and activates transcription in a stress-dependent manner.[5−7] Transcripts regulated by Hsf1 in the stress response include molecular chaperones that suppress protein aggregation and assist protein folding[8] and proteins involved in cell survival, such as proteolysis, signal transduction, cytoskeleton, and apoptosis regulators.[9−12]

The function of Hsf1 is controlled by its oligomeric state. Hsf1 is mostly composed of intrinsically disordered regions consisting of a regulatory domain (RegD) and a C-terminal transactivation domain (CTAD) and has a DNA-binding domain (DBD) and the leucine-zipper domains (LZ1−3 and LZ4) as structural domains (Figure 1A).[13] Under normal conditions, Hsf1 is maintained in a monomeric state by forming a complex with molecular chaperones, such as heat shock protein (Hsp) 70 and Hsp90, in the cytosol.[14−17] It has been proposed that under stress conditions, chaperones dissociate from Hsf1 to rescue the misfolded proteins, and Hsf1 accumulates in the nucleus to form oligomers.[18−20] It was also proposed that Hsf1 itself has the ability to regulate its own oligomeric state and maintain its monomeric state through intramolecular interactions between LZ1−3 and LZ4.[21] Purified Hsf1 oligomerizes in response to elevated temperatures, indicating that Hsf1 itself can function as a thermosensor.[14,22,23] The Hsf1 oligomer binds to the heat shock element (HSE) DNA located in the promoter region upstream of the gene encoding chaperones and promotes transcription.[20,24,25] Thus, the monomer−oligomer transition of Hsf1 is critical for transcriptional regulation in HSR. While this HSR system is responsible for protecting normal cells from stress, it is also known to be closely related to pathophysiology

Received: August 24, 2022
Revised: November 12, 2022
Published: December 9, 2022

https://doi.org/10.1021/acs.biochem.2c00492
Biochemistry 2022, 61, 2897−2908

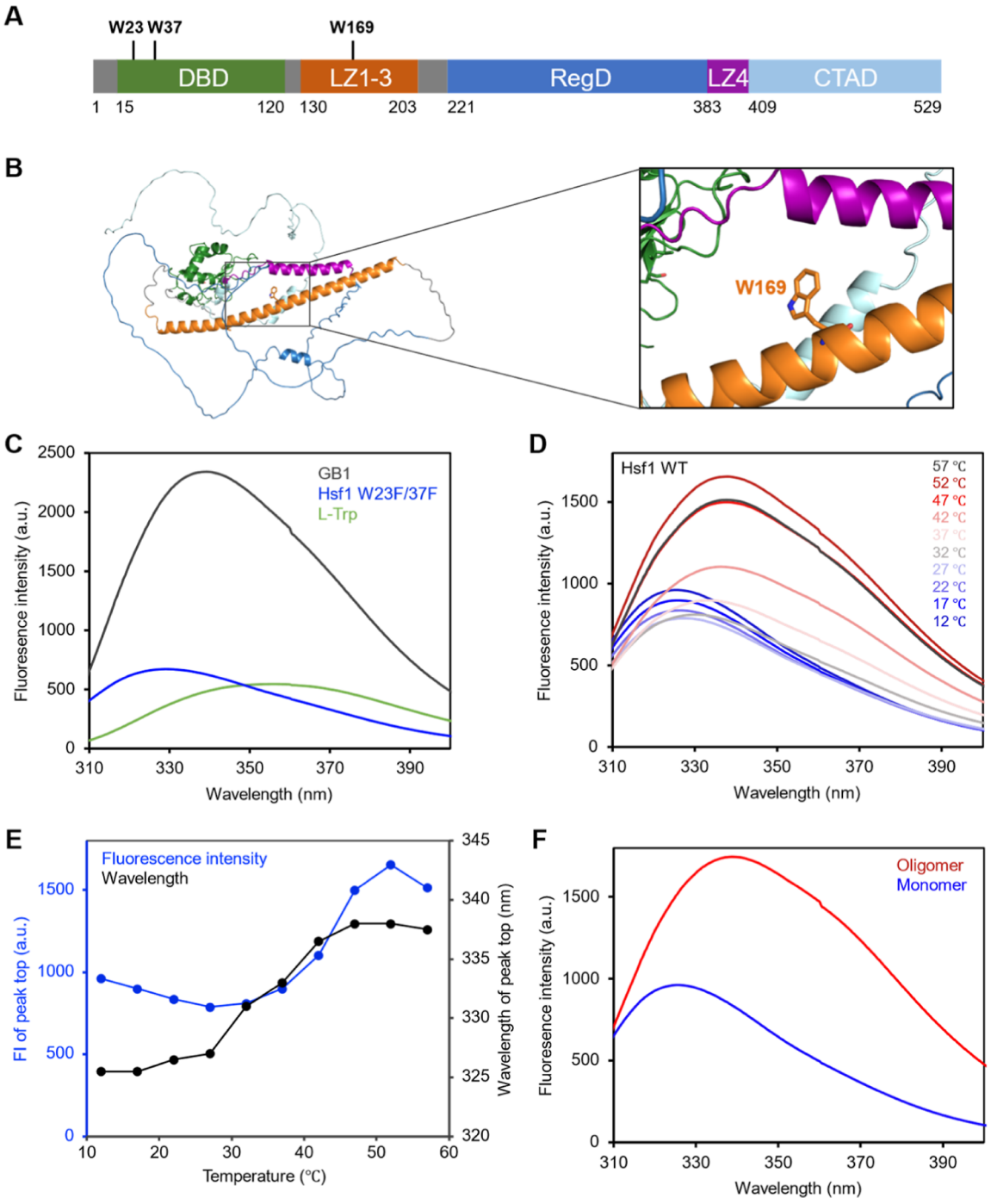

Figure 1. Monitoring conformational changes and oligomerization of Hsf1 by observing Trp fluorescence. (A) Domain organization and location of tryptophan residues in Hsf1. The abbreviations used are as follows: DBD, DNA-binding domain; LZ1-3, leucine-zipper domain-1−3; RegD, regulatory domain; LZ4, leucine-zipper domain-4; CTAD, C-terminal transactivation domain. (B) Molecular structure of HSF1 estimated by the AlphaFold2 and close-up view of the structure around Trp169. (C) Trp fluorescence spectra of Hsf1 W23F/W37F monomer, GB1, and L-Trp solution at 12 °C. (D) Trp fluorescence spectra of the Hsf1 monomer at varying temperatures from 12 to 57 °C. (E) Transition of fluorescence intensity and wavelength at the peak top in the temperature change measurement. (F) Fluorescence spectra of Hsf1 monomer (blue) and oligomer (red) at 12 °C.

such as tumorigenesis.[26,27] Moreover, a decrease in the HSR amplitude is associated with neurodegenerative diseases.[28] These facts showing the relevance of Hsf1 in multiple diseases suggest the importance of Hsf1 regulation in HSR.

Several structural studies have been conducted to elucidate the molecular mechanism of Hsf1-mediated HSR. A model structure of the human Hsf1 trimer was obtained using the crystal structure of *Chaetomium thermophilum* Skn7 (160−209) that is homologous to the LZ1−3 domain of Hsf1, suggesting that LZ1−3 forms a trimer.[29] Moreover, the HSE DNA recognition mechanism was clarified using the crystal structures of the DBD−HSE complex.[29−31] These structural studies highlighted the detailed mechanisms by which the Hsf1 oligomer recognizes HSE. On the other hand, the mechanism

https://doi.org/10.1021/acs.biochem.2c00492
Biochemistry 2022, 61, 2897−2908

by which Hsf1 alters its oligomeric state in response to heat is poorly understood. Several biochemical studies have implied that Hsf1 acts as a thermosensor by controlling temperature-dependent LZ1−3 and LZ4 interactions.[21,22,24,32,33] It has been reported that Hsf1 forms oligomers by deletion or substitution of LZ4, which disrupts the intramolecular interaction between LZ4 and LZ1-3,[21,32,33] leading to the hypothesis that the Hsf1 monomer is maintained by the intramolecular interaction between LZ1−3 and LZ4 under normal conditions, but under stress, this interaction is dissolved to allow intermolecular interaction among LZ1−3.[21,24] However, the transition mechanism from the monomer to the oligomer due to a change in the interaction between LZ1−3 and LZ4 has not been fully examined.

In this study, we aimed to uncover the mechanism of the Hsf1 heat response by investigating the temperature-dependent conformational transition of Hsf1 using solution biophysical methods. The fluorescence derived from Trp169 located at LZ1−3 (Figure 1A,B) was monitored to track the temperature-dependent conformational changes and oligomerization of Hsf1. Moreover, in combination with its model fitting analysis, 8-anilino-1-naphtalene sulfonic acid (ANS) fluorescence, nuclear magnetic resonance (NMR), and circular dichroism (CD) spectroscopy, we found that the oligomer, the active form of Hsf1, is formed via the monomer of the open conformation, in which LZ1−3 dissociates from LZ4 at elevated temperatures. Furthermore, this conformational change to the open state is coupled with unfolding of the helix structure. This study revealed the existence of a monomeric open conformation of Hsf1 prior to oligomerization. This open/closed conformational change can be a key reaction for the regulation of its oligomeric state, as well as interactions with other regulators, such as molecular chaperones.

MATERIALS AND METHODS

Expression and Purification of Protein Samples. The human Hsf1 (1−529), Hsf1 DBD (1−120), Hsf1 LZ4 (367−446), and Hsf1 W23F/W37F expression constructs were cloned into a pET21b vector (Cat. no. 69741-3CN; Novagen, Madison, Wisconsin, USA) and fused to GB1-His^6 tags at the HRV3C N-terminus of the protease cleavage site. Hsf1 DBD, Hsf1 LZ4, and Hsf1 W23F/W37F were constructed through site-directed mutagenesis using the PrimeSTAR Mutagenesis Basal Kit (Cat. no. R046A; Takara Bio, Shiga, Japan). All the expression constructs were transformed into BL21(DE3) cells. The cells were grown in the Luria−Bertani medium at 37 °C in the presence of ampicillin (50 μg mL^{-1}). Subsequently, protein expression was induced by adding 0.5 mM isopropyl-β-D-1-thiogalactopyranoside at OD_{600} ∼0.6, followed by a 12−16 h incubation at 18 °C. Then, the cells were harvested at OD_{600} ∼3.0, resuspended in a lysis buffer containing 50 mM Tris−HCl (pH 8.0) and 500 mM NaCl, disrupted by a sonicator, and centrifuged at 18,000 rpm for 30 min. The supernatant fraction containing Hsf1 was purified using a Ni-NTA Sepharose column (Cat. no. 30210; QIAGEN, Hilden, Germany). Additionally, the GB1-His^6 tag was removed using a HRV3C protease at 4 °C (incubation for 16 h), post which the cleaved Hsf1 was applied onto a HiTrap Q HP anion-exchange column (Cat. no. 17115401; Cytiva, Marlborough, MA, USA), pre-equilibrated with 25 mM HEPES/NaOH (pH 7.5), 5 mM $MgCl_2$, 10% glycerol, 20 mM NaCl, and eluted with a linear gradient of 20−500 mM NaCl. Hsf1 oligomers and Hsf1 monomers were eluted separately through anion-exchange purification. Hsf1 oligomers were further purified by gel filtration using a Superdex 200 pg 16/600 column (Cat. no. 28989335; Cytiva) equilibrated with a solution containing 25 mM HEPES/KOH (pH 7.2) and 150 mM KCl. Finally, protein concentrations were determined spectrophotometrically at 280 nm using the corresponding extinction coefficient.

Fluorescence Spectroscopy. Fluorescence measurements were performed using a JASCO FP-8300 spectrofluorometer and using solutions prepared in 25 mM HEPES/KOH (pH 7.2) and 150 mM KCl. The concentrations of Hsf1, GB1, and L-Trp amino acid (Cat. no. 206-03381; Wako, Osaka, Japan) solution were all 3.0 μM. The unpolarized emission spectra of tryptophan were recorded between 300 and 450 nm using an excitation wavelength of 295 nm and a scan speed of 200 nm/min. The emission spectra of ANS (Sigma-Aldrich, St Louis, USA) were recorded between 400 and 700 nm using a 375 nm excitation wavelength and a scan speed of 200 nm/min. The concentration of ANS was 50 μM. Fluorescence resonance energy transfer (FRET) spectra were recorded between 300 and 700 nm using an excitation wavelength of 295 nm and a scan speed of 200 nm/min. The excitation and emission slit widths were both set to 5 nm. Each spectrum represents an integration of three consecutive scans.

Fitting Procedure of Fluorescence Spectra. The fluorescence spectral data were analyzed using a mathematical model and a global fitting algorithm. The oligomeric number of Hsf1 was formulated as a trimer based on its crystal structure.[29−31] The mathematical model assumes a three-state transition (3M ↔ 3I ↔ O), written as

$$K_{MI}[M] = [I] \tag{1}$$

$$K_{IO}[I]^3 = [O] \tag{2}$$

where K_{MI} and K_{IO} are the association constants for the reactions M ↔ I and I ↔ O, respectively. [...] denotes that the concentration of Hsf1 in each state is normalized by the total concentration of Hsf1 in the sample. The temperature dependence of the association constants is written as

$$K_{MI} = \exp\left(-\frac{\Delta H_{MI}}{RT}\left(1 - \frac{T}{T_{m,MI}}\right)\right) \tag{3}$$

$$K_{IO} = \exp\left(-\frac{\Delta H_{IO}}{RT}\left(1 - \frac{T}{T_{m,IO}}\right)\right) \tag{4}$$

where R is the gas constant, $T_{m,MI}$ and $T_{m,IO}$ are the midpoint temperatures of the reactions M ↔ I and I ↔ O, respectively, and ΔH_{MI} and ΔH_{IO} are the molar enthalpy changes of the transition at $T_{m,MI}$ and $T_{m,IO}$, respectively. Combining eqs 1 and 2 with the mass conservation law in the monomer unit yields the following equation

$$3K_{IO}K_{MI}^3[M]^3 + (K_{MI} + 1)[M] = 1 \tag{5}$$

The analytical solution for eq 5 was obtained using Mathematica.

To fit the mathematical model to the fluorescence data, the thermodynamic parameters ΔH_{MI}, ΔH_{IO} $T_{m,MI}$, and $T_{m,IO}$ were numerically solved using an iterative method. Their initial values were set, [M], [I], and [O] were calculated at each temperature according to eqs 1−5, and the matrix of the

https://doi.org/10.1021/acs.biochem.2c00492
Biochemistry 2022, 61, 2897−2908

population fraction C was the output. The matrix of the pure component spectra S of Hsf1 in the M, I, and O states was calculated using the classical least-squares method[34]

$$S = (C^{T}C)^{-1}CD \quad (6)$$

where D is the matrix of the measured fluorescence data. The 2-norm of the error $E = |CS - D|_2$ was minimized by repeating the calculation with different initial parameter values, and the solutions obtained for the parameters were used to compare the experimental data.

SEC−MALS Experiments. Size exclusion chromatography with multi-angle light scattering (SEC−MALS) was performed using a DAWN HELEOS8+ (Wyatt Technology Corporation, Santa Barbara, CA, USA), a high-performance liquid chromatography pump LC-20AD (Shimadzu, Kyoto, Japan), a refractive index detector RID-20A (Shimadzu), and a UV−vis detector SPD-20A (Shimadzu), which were located downstream of the Shimadzu liquid chromatography system connected to a PROTEIN KW-803 gel filtration column (Cat. no. F6989103; Shodex, Tokyo, Japan). Differential RI (Shimadzu) downstream of MALS was used to determine the protein concentrations. The running buffer used contained 25 mM HEPES/KOH (pH 7.2) and 150 mM KCl. Approximately 100 μL of the sample was injected at a flow rate of 1.0 mL min^{-1}. Data was then analyzed using ASTRA version 7.0.1 (Wyatt Technology Corporation). Molar mass analysis was also performed over half of the width of the UV peak top height. After 30 min, incubation at 12, 27, and 42 °C, 100 μL of 50 μM Hsf1 monomer sample was injected.

NMR Spectroscopy. NMR samples were prepared in 25 mM potassium phosphate buffer (pH 7.2), 150 mM KCl, 0.05% NaN_3, and 7% D_2O for one-dimensional (1D) ^{19}F-NMR experiments or 20 mM MES (pH6.5), 100 mM NaCl, 5 mM $CaCl_2$, 0.02% NaN_3, and 7% D_2O for 1D ^{1}H-NMR experiments. The concentration of Hsf1 was 100 μM, and the concentrations of Hsf1 DBD and Hsf1 ΔDBD were 50 μM. The ^{19}F-NMR experiments were performed at 12 °C. ^{19}F-NMR spectra and ^{1}H-NMR spectra were obtained with a Bruker AVANCE NEO 800 MHz spectrometer (Bruker, Billerica, MA) using a CPTCI ^{1}H/^{19}F−^{13}C/^{15}N proton-optimized triple resonance cryoprobe. The 1D ^{19}F-NMR experiments were recorded with a data size of 131,072 complex points, an acquisition time of 367 ms, and 32,768 scans per experiment. The 1D ^{1}H-NMR experiments were recorded with a data size of 32,768 complex points, an acquisition time of 1310 ms, and 128 scans per experiment. The spectra were processed using Bruker TOPSPIN version 3.6.2.

CD Spectroscopy. The CD spectra were recorded using a JASCO J-1500 CD spectrometer (Tokyo, Japan) with 1 mm path length cuvettes at 22 °C in 10 mM potassium phosphate buffer (pH 7.2). Each spectrum represents an integration of three consecutive scans from 190 to 260 nm at 1.0 nm intervals, with a scan speed of 20 nm/min. The concentrations of Hsf1 and LZ4 were 1.5 μM and 10.0 μM, respectively. The helix content was predicted using BeStSel.[35]

DLS Experiments. Dynamic light scattering (DLS) was performed using a Zetasizer Nano ZS (ZEN3600, Malvern Instrument, UK) equipped with a 633 nm red laser and 173° scattering angle. "Size" and "Protein" were selected as the measurement type and the material type, respectively. For each sample, the measurement was repeated three times. After the diffusion of a particle moving under Brownian motion was measured, the Zetasizer software version 8.02 converted the diffusion to a size and generated size intensity distributions using Stokes−Einstein relationship with a refractive index of 1.45 nD and a dynamic viscosity of 0.6262 cP. Gaussian fitting was then used to extract the size mean. The analysis was performed with the lower and upper size limits set to 0.4 and 10,000 nm, respectively. The Hsf1 monomer was prepared in 25 mM HEPES/KOH (pH 7.2) and 150 mM KCl, and its concentration was 5 μM. Data were acquired after 30 min incubation at 12, 25, and 42 °C in the cuvette.

Simulations. All-atom MD simulations were performed with the CHARMM36m force field[36] using LAMMPS software.[37] Given an open conformation of Hsf1 at high temperatures, the isolated model of the Hsf1 LZ4 was employed to investigate the helical unfolding. The molecular structures of Hsf1 were estimated by AlphaFold 2 (AF2),[38] and then the estimated structure of LZ4 regions were extracted and used as the initial configurations. The isolated model of LZ4 was placed in a periodic simulation box and solvated by adding water. The salt concentration was set to 150 mM KCl, and the corresponding numbers of K^+ and Cl^- ions were added. After the steepest-descent energy minimization, the systems were relaxed for 100 ps at a temperature of 355 K and a pressure of 1 atm, followed by production runs for 500 ns in the NPT ensemble at a temperature of 355 K. The temperature was maintained using a Nosé−Hoover thermostat,[39,40] and the pressure was controlled using a Parrinello−Rahman barostat.[41,42] The non-bonded interactions were calculated with a cutoff distance of 1.2 nm, and the particle−particle particle−mesh method[43] was used to calculate long-range electrostatic interactions. The equations of motion were integrated using the Verlet algorithm[44] with a time step of 2 fs, along with the SHAKE algorithm,[45] to constrain the bond lengths to hydrogen. The root-mean-square deviations (rmsd) for Cα atoms were calculated with respect to the starting structure for the system using the MD simulation trajectories over 500 ns. The secondary structure of the protein structures was determined by DSSP[46] to probe the conformational transition over time.

RESULTS

Tracking Temperature-Dependent Conformational Changes and Oligomerization of Hsf1 by Trp-Fluorescence Spectroscopy. To obtain structural information of Hsf1 in the monomeric form, we first obtained the AlphaFold2 (AF2) model of Hsf1 monomer.[38] The AF2-predicted structure of the Hsf1 monomer showed that Hsf1 has a closed conformation in which LZ1-3 and LZ4 are associated with each other (Figure 1B). The structural model showed that Trp169, one of the three tryptophan residues (Trp23/Trp37/Trp169) in Hsf1, is located in LZ1−3 and faces toward LZ4 (Figure 1B). To test whether the conformational changes in LZ1-3 and LZ4 can be tracked by observing fluorescence changes of Trp169, we compared the fluorescence spectra of Hsf1 W23F/W37F with that of L-Trp amino acid solution that is exposed in the solvent and immunoglobulin binding domain of protein G (GB1) that has one Trp residue fixed in the core of the protein[47] (Figures 1C and S1A). The fluorescence spectra of Hsf1 W23F/W37F showed that the peak top wavelength is slightly shorter than GB1, suggesting that the Trp169 of Hsf1 is in a hydrophobic environment. This result is consistent with the AF2-predicted structure of Hsf1 in which Trp169 is surrounded by hydrophobic residues (Figure S2A). The fluorescence intensity is larger than that of L-Trp solution

https://doi.org/10.1021/acs.biochem.2c00492
Biochemistry 2022, 61, 2897−2908

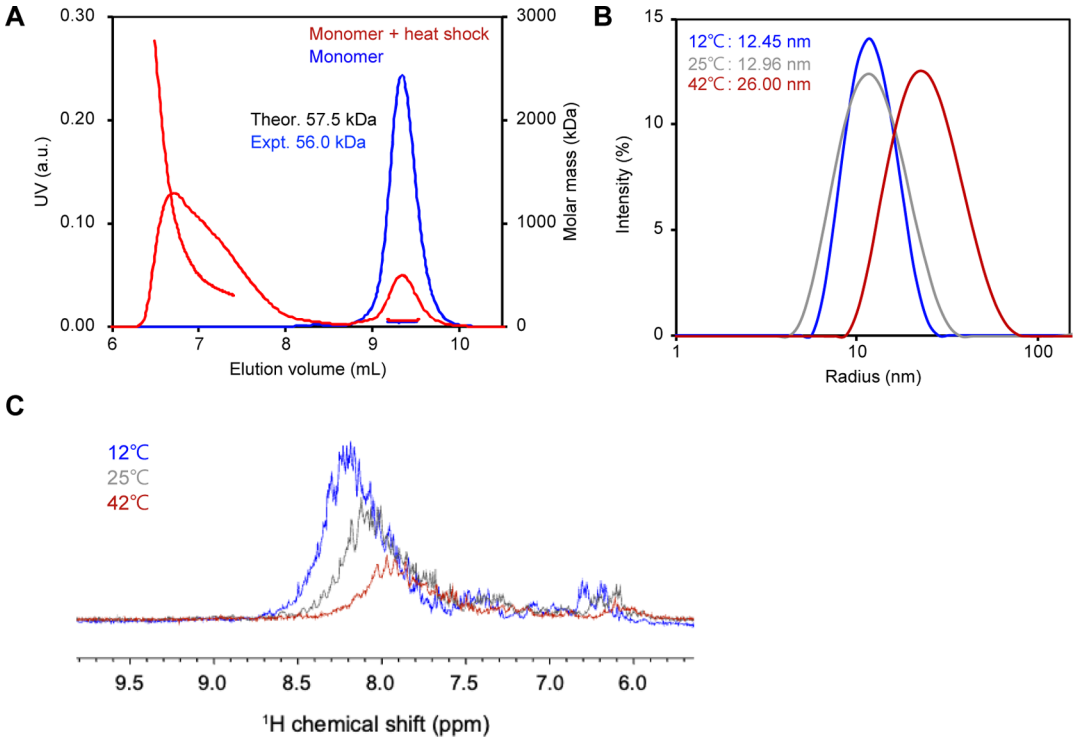

Figure 2. Monitoring conformational changes and oligomerization of Hsf1 by observing Trp fluorescence. (A) SEC−MALS of the Hsf1 monomer at room temperature (blue) and after heat shock at 42 °C (red). (B) DLS analysis of the Hsf1 monomer at 12 °C (blue), 25 °C (gray), and 42 °C (red). (C) ^{1}H NMR spectra of the Hsf1 monomer at 12 °C (blue), 25 °C (gray), and 42 °C (red).

but smaller than that of GB1, indicating that the Trp169 of Hsf1 has relatively high mobility compared to the rigid folded proteins (Figure 1B). This result suggests that the structure of LZ1−3 and LZ4 is dynamic in solution. Collectively, the above results showed that the Trp fluorescence can be exploited to probe conformational state and changes of Hsf1 LZ1−3 and LZ4 in solution.

To track the conformational transition from the monomer to the oligomer, we monitored the temperature dependence of tryptophan fluorescence in the monomer of Hsf1 full length (residues: 1−529) (Figure 1D). Hsf1 was separated into monomer and oligomer fractions by purification with SEC, and the monomer fraction was used for fluorescence measurement. Both the wavelength and intensity of the fluorescence peak showed significant changes with temperature change (Figure 1D,E). The plot of the peak top wavelength with respect to the temperature showed that the peak top stayed around 327 nm in the temperature range from 12 to 27 °C and gradually red-shifted toward 337 nm in the temperature range from 27 to 42 °C. The fluorescence spectra of the Hsf1 monomer and oligomer showed that the maximum wavelength of the oligomer was red-shifted from that of the monomer (Figure 1F). The wavelength of the oligomer fraction was 338.5 nm, which is close to the fluorescence maximum wavelength at 42−57 °C (Figure 1D,E), implying that the red-shift coincides with Hsf1 oligomerization. The red shift of the fluorescence peak generally reflects an environmental change toward hydrophilic conditions.[48] This is consistent with the AF2-predicted structure, in which Trp169 of Hsf1 forms a hydrophobic cavity in the monomer, while it is exposed to the solvent in the oligomer (Figure S2A,B). The oligomeric state of Hsf1 at each temperature was evaluated by SEC−MALS, DLS, and 1D ^{1}H-NMR experiments (Figures 2A−C and S3). SEC−MALS showed that Hsf1 stays mostly as a monomer at room temperature and up to 27 °C whereas forms an oligomer after heat shock at 42 °C (Figures 2A and S3). In the DLS experiments, the radius of Hsf1 was estimated to be 12∼13 nm at 12 and 25 °C, while the radius increased to 26 nm at 42 °C, indicating the formation of oligomers at the elevated temperature (Figure 2B). Formation of Hsf1 oligomers at 42 °C was further corroborated by 1D ^{1}H-NMR experiments in which the intensity of Hsf1 resonances decreased as the temperature increased (Figure 2C). Decreased resonance intensity at higher temperature can be explained by line broadening owing to oligomerization that causes slower tumbling. Collectively, these results showed that Hsf1 exists mostly as a monomer at 12 and 25 °C and forms an oligomer at 42 °C, which is consistent with previous studies showing that Hsf1 oligomerizes around 42 °C.[14,22,23] Therefore, we concluded that the red-shifted Trp fluorescence at higher temperature reflects Hsf1 oligomerization.

Next, temperature-dependent changes in the Trp fluorescence intensity at maxima were evaluated to track the conformational changes of Hsf1 (Figure 1D). Note that the fluorescence intensity reflects the local mobility of the Trp residues. The fluorescence intensity decreased from 12 to 27 °C and increased from 27 to 52 °C (Figure 1D,E). Considering that the intensity of the fluorescence maxima was higher for the oligomer than for the monomer (Figure 1F), an increase in the fluorescence intensity in the spectrum above 27 °C can be attributed to oligomerization. On the contrary, the fluorescence intensity decreased as the temperature increased from 12 to 27 °C (Figure 1D,E). Such biphasic changes in the fluorescence intensity are characteristic of state changes through intermediates and indicate the existence of intermediates in response to heat. Note that this biphasic

https://doi.org/10.1021/acs.biochem.2c00492
Biochemistry 2022, 61, 2897−2908

transition of Trp fluorescence was not seen in the control experiment using GB1 (Figure S1). Although the fluorescence intensity of GB1 slightly decreased as the temperature increased, the intensity change in GB1 spectra was much less significant than in Hsf1 spectra (Figure S1B,C). Furthermore, the peak top wavelength of GB1 Trp fluorescence spectra remained almost unchanged even at high temperature (Figure S1B,D).

Characterization of Intermediate Monomeric State by Model Fitting Analysis. To investigate the transition mechanism from the monomeric state to the oligomeric state through the intermediate state, we structurally characterized the intermediate state of Hsf1 by analyzing the fluorescence spectral data using a mathematical model and global fitting simulation. Singular value decomposition (SVD) analysis of the fluorescence spectra suggested that at least three components were present (Figure S4). The mathematical model assumes that Hsf1 has three states: the initial monomeric state (M), the monomeric intermediate state (I), and the oligomeric state (O). This model can be written as

$$M \leftrightarrow I \leftrightarrow O$$

Figure 3A shows the experimental plot and fitting curve of the temperature dependence of fluorescence peak intensity. The fitting curve reproduced the experimental results well, indicating that the three-state model explained the experimental data well. The fitting analysis provided the population fractions of the three states and revealed that the major population fractions of Hsf1 transitioned from the M state to the I state around 20 °C and from the I state to the O state around 40 °C (Figure 3B). This is consistent with the results from SEC−MALS and DLS showing that a majority of Hsf1 became oligomeric at 42 °C (Figure 2A,B) and also suggests that the I state can be a major conformation at approximately 37 °C, the normal intracellular temperature. To obtain structural information on the intermediate state, we computed the component spectra of Hsf1 in the three states (Figure 3C). The computed spectra of Hsf1 in the M and O states exhibited a peak fluorescence at 324.5 and 338.5 nm, respectively. These computed fluorescence spectra corresponded well with those obtained experimentally for the monomer and oligomer Hsf1 (Figure 1F). Interestingly, Hsf1 in the I state showed a peak fluorescence at 331.5 nm, indicating that the peak position of the fluorescence spectrum in the I state was red-shifted from that in the M state. Furthermore, the peak intensity in the I state was weaker than that in the M state. The peak red shift and intensity reduction in the tryptophan fluorescence spectrum of the I state can be interpreted as solvent exposure and increased the mobility of tryptophan residues, respectively.[48]

Model fitting analysis showed that the tryptophan residues in the I state have increased mobility compared to those in the M state. To confirm whether the I state reflects the conformational state of LZ1−3 and LZ4, we selectively observed fluorescence from Trp169 in LZ1−3 by substitution of Trp23 and Trp37 with phenylalanine in the DBD. As a result, the fluorescence intensity became minimal at 27 °C, which coincided with the intensity change of Hsf1 WT (Figure 4A,B). Therefore, the decrease in fluorescence intensity was due to the increased mobility of Trp169 located in LZ1−3. Focusing on the wavelength of the fluorescence maxima of the Hsf1 W23F/W37F mutant, a red shift was observed in the region from 12 to 27 °C (Figure 4A,B). Because LZ4 is an

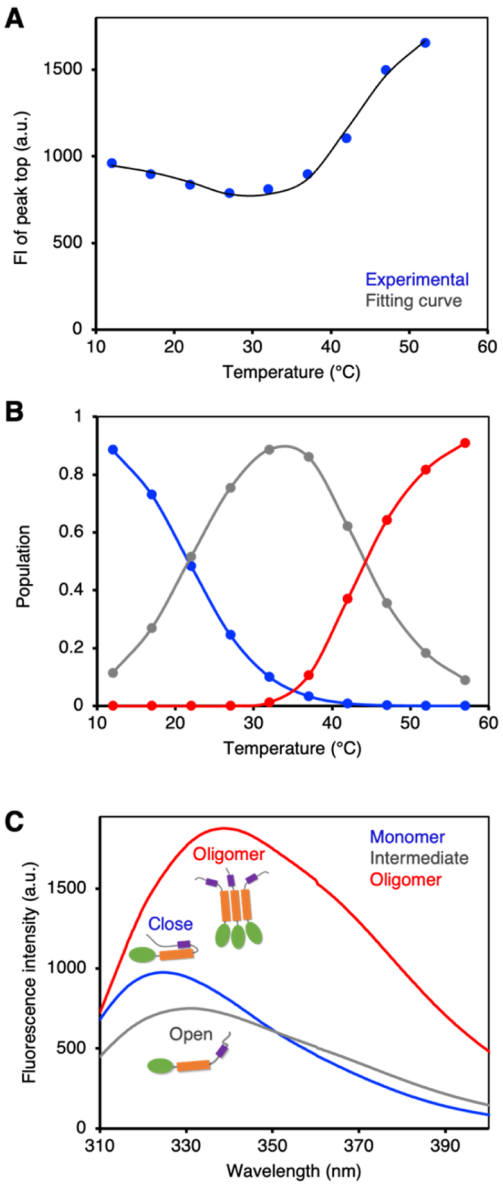

Figure 3. Model fitting analysis of Trp fluorescence measurement. (A) Experimental plot and fitting curve of the temperature dependence of fluorescence peak intensity. (B) Populational fractions of the three states from the fitting analysis. (C) Computed component spectra of Hsf1 in the three states.

amphiphilic helix and its hydrophobic side faces LZ1−3 in the structural prediction of LZ4 by Netwheels and AF2[38,49] (Figure 4C,D), it is suggested that this red shift reflects a weakening of the hydrophobic interaction between LZ1−3 and LZ4. Note that SEC-MALS and DLS results showed that Hsf1 was mostly present as a monomer around 27 °C (Figures 2B and S3), suggesting that the intermediate should be in a monomeric state. Therefore, Trp fluorescence measurements and model fitting analysis demonstrated that Hsf1 oligomerizes through the monomeric intermediate in which the mobility of Trp169 is increased and the intramolecular interaction between LZ1−3 and LZ4 is dissolved.

Tracking the Temperature-Dependent Dissolution of the Hydrophobic Cavity of Hsf1. Next, we aimed to further investigate the structure of the Hsf1 intermediate. Fluorescence measurement and model fitting analysis suggested the

https://doi.org/10.1021/acs.biochem.2c00492
Biochemistry 2022, 61, 2897−2908

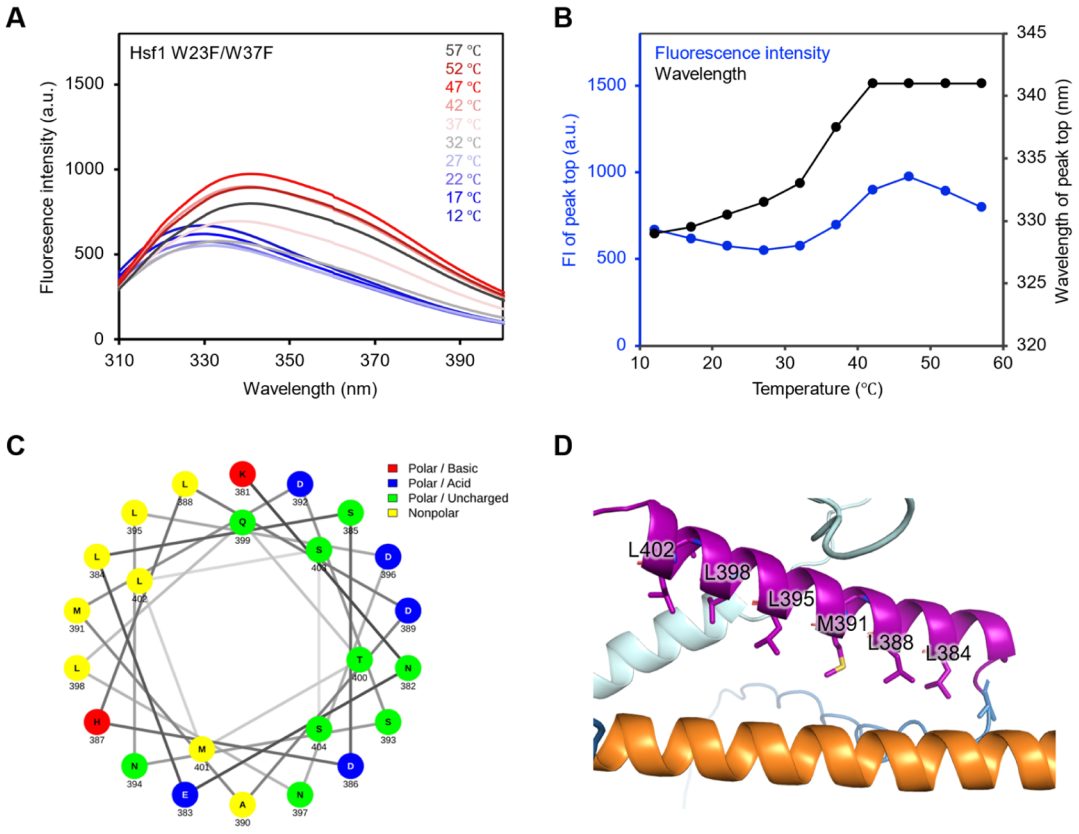

Figure 4. Monitoring the Trp169 fluorescence of Hsf1. (A) Trp fluorescence spectra of Hsf1 W23F/W37F at varying temperatures from 12 to 57 °C. (B) Transition of fluorescence intensity and wavelength at the peak top in the temperature change measurement. (C) Helical wheel and net projections created using NetWheels. (D) Close-up view of the structure around LZ1−3 (orange) and LZ4 (magenta) estimated by AlphaFold2. Tracking the temperature-dependent dissolution of the hydrophobic cavity of Hsf1.

existence of the intermediate open conformation in which the intramolecular interaction between LZ1−3 and LZ4 is dissolved. To support this, the hydrophobic cavity formed between LZ1−3 and LZ4 (Figure S2A) was evaluated by fluorescence measurements of ANS, a compound whose fluorescence maxima increased significantly and its wavelength blue-shifted under hydrophobic conditions compared to that in an aqueous solution.[50] Trp fluorescence measurements suggested that at lower temperatures, the interaction between LZ1−3 and LZ4 in the closed conformation forms a hydrophobic cavity (Figures 1, 3, 4 and S2A), whereas at higher temperatures, the transition toward the open conformation disrupts the hydrophobic cavity and is thus expected to alter ANS fluorescence properties. ANS was added to the Hsf1 monomer, and temperature-dependent changes in ANS fluorescence were monitored. Because the affinity between ANS and the target protein decreased in a temperature-dependent manner,[51] it was difficult to evaluate the conformational change of Hsf1 with the disruption of hydrophobic cavities from the linear decrease in ANS-derived fluorescence intensity in the temperature range from 12 to 37 °C (Figure 5A,B). On the contrary, change in the fluorescence maximum wavelength showed a biphasic profile in which the fluorescence maxima red-shifted in the temperature region from 12 to 27 °C but blue-shifted in the temperature region from 27 to 52 °C (Figure 5A,B), suggesting that the ANS fluorescence wavelength reflects information about the intermediate. Note that the inflection points around 27 °C roughly coincides with that observed in the Trp fluorescence analysis (Figure 1E). The red shift of ANS fluorescence suggested that the environment of the ANS binding site on Hsf1 became gradually hydrophilic, suggesting that the hydrophobic cavity, most probably the cavity formed between LZ1−3 and LZ4, of Hsf1 was disrupted at 27 °C. In the temperature region from 27 to 52 °C, the fluorescence maximum wavelength was blue-shifted (Figure 5A,B). Thus, changes in the high-temperature region may be due to the binding of ANS to the newly formed hydrophobic cavities by oligomerization (Figure S2B). Notably, ANS-derived fluorescence at 12 °C was 145 a.u. at 470.5 nm for Hsf1 full length and 9 a.u. at 491.5 nm for the isolated Hsf1 DBD (Figure S5A,B), suggesting that ANS barely interacts with DBD. This indicates that the changes in ANS fluorescence reflect the conformational changes in the C-terminal region, including LZ1−3 and LZ4 in full-length Hsf1.

To determine whether the temperature-dependent changes in ANS-derived fluorescence reflect the conformational change between LZ1−3 and LZ4, we investigated the binding site of ANS for Hsf1 by ^{19}F NMR for [5-^{19}F-Trp] Hsf1, in which three Trp residues (Trp23, Trp37, and Trp169) were substituted by 5-^{19}F-Trp. Three ^{19}F NMR signals were observed, indicating that each of the three tryptophan residues in Hsf1 (Trp23, Trp37, and Trp169) exhibited a single signal (Figure 5C). To assign the resonances, ^{19}F NMR was performed for Hsf1 DBD containing Trp23 and Trp37 and Hsf1 ΔDBD containing Trp169. Two ^{19}F NMR signals for Hsf1 DBD were observed at −123.2 ppm and −124.6 ppm, and only one ^{19}F NMR signal for Hsf1 ΔDBD was observed at −125.3 ppm (Figure 5C). Therefore, the ^{19}F NMR signal at

https://doi.org/10.1021/acs.biochem.2c00492
Biochemistry 2022, 61, 2897−2908

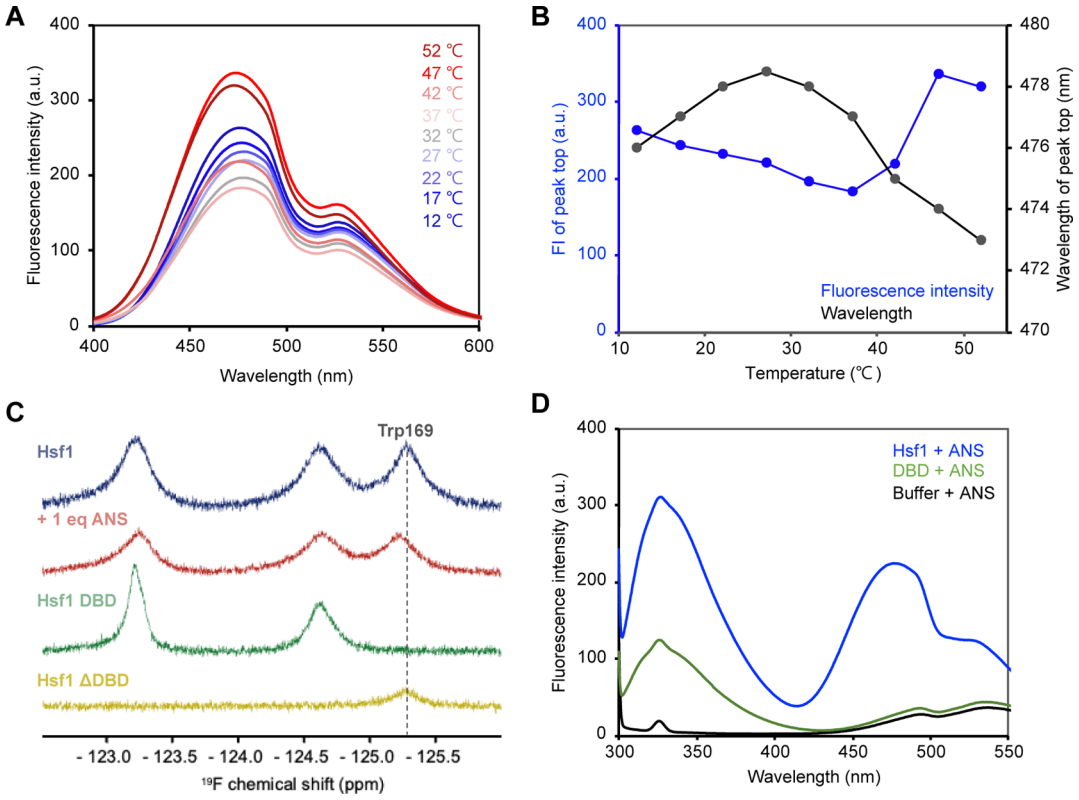

Figure 5. Tracking the collapse of the hydrophobic cavity of Hsf1 by ANS fluorescence measurements. (A) ANS fluorescence spectra mixed with Hsf1 at varying temperatures from 12 to 52 °C. (B) Transition of fluorescence intensity and wavelength at the peak top in the temperature change measurement. (C) ^{19}F NMR spectra of 5-^{19}F-Trp-labeled Hsf1 monomer (blue), Hsf1 monomer + 1 equiv ANS (red), Hsf1 DBD (green), and Hsf1 deltaDBD (ΔDBD) (yellow) at 12 °C. The signal from Trp169 was assigned from comparison of spectra of Hsf1, Hsf1 DBD, and Hsf1 ΔDBD. (D) Upon tryptophan excitation at 295 nm, FRET between ANS and Hsf1 is characterized by the apparition of a signal at 475 nm (blue). Spectra of mixed samples of Hsf1 DBD and ANS under the same conditions (green). Emission spectra of ANS alone are colored in black. Since FRET was observed only in Hsf1, it was indicated that ANS binds to the hydrophobic cavity formed between LZ1−3 and LZ4 in Hsf1.

−125.3 ppm was assigned to the Trp169-derived signal located in the LZ1−3 region. This ^{19}F NMR signal of Trp169 showed chemical shift perturbation by the addition of 1 equiv of ANS (Figure 5C), showing that ANS interacts with Trp169 located in the hydrophobic cavity.

To further support ANS binding to the hydrophobic cavity, Trp-ANS FRET was performed. When a mixed sample of Hsf1 and ANS was excited at 295 nm, near the Trp excitation wavelength at 12 °C, ANS fluorescence was observed, indicating ANS binding around the Trp of Hsf1 (Figure 5D). Trp-ANS FRET was not observed in the mixed samples of DBD and ANS (Figure 5D). These ^{19}F-Trp NMR and FRET analyses showed that ANS binds to the hydrophobic cavity formed between LZ1−3 and LZ4 in a closed conformation. Thus, monitoring the dissolution of the hydrophobic cavity by ANS fluorescence supports that the Hsf1 intermediate is in an open conformation in which LZ1−3 and LZ4 are dissociated.

Secondary Structure in the Formation of the Intermediate. Our results show that Hsf1 forms a monomeric open state in which LZ1-3 and LZ4 are dissociated at higher temperature and thus suggest that the helical structures of leucine zippers (LZs) can be destabilized in the open conformation. To investigate the secondary structure of Hsf1 in the monomeric open conformation, we measured CD spectroscopy at varying temperatures. Measurements of CD spectra of Hsf1 at 12 °C showed a minimum ellipticity at 207 nm, characteristic of a protein with a high α-helical content (Figure 6A). The α-helical content calculated from this CD spectrum using the BeStSel program[35] was 27.2%, which was in good agreement with the α-helical content of 28.4% calculated from the AF2 predictive structure (Figures 6A,B, and S6A,F,G). The negative ellipticity in the region from 205 to 230 nm decreased and the α-helical contents were perturbed from 27.2% at 12 °C to 19.6% at 52 °C as the temperature increased (Figures 6A,B, and S6A−G), indicating the unfolding of the helical structure at elevated temperatures. The CD spectra of LZ4 alone showed a minimum ellipticity at 201 nm, and the α-helical content was calculated to be only 1.1% (Figures 6C and S6G), showing that the isolated LZ4 is mostly unfolded. The data indicate that the helical structures of LZ1−3 and LZ4 are stabilized at closed conformation, but LZ4 unfolds without support from LZ1−3 at open conformation and oligomeric state. Note that the unfolding of LZ4 is also supported by MD simulation at 355 K (Figure S7). The trajectory of rmsd from the initial structure showed that the rmsd of LZ4 gradually increased. The trajectory of helix content showed that the helix content in the isolated LZ4 gradually decreased over time (Figure S7). Thus, the data from MD simulations support the idea that LZ1−3 and LZ4 are destabilized and undergo unfolding in the open conformation at higher temperature. Notably, the unfolding of helical structures in Hsf1 at higher temperatures was not reversible and CD spectra changed slightly when the temperature was decreased from 52 to 12 °C (Figure S6H), indicating that heat-induced Hsf1 oligomerization is irreversible and is consistent

https://doi.org/10.1021/acs.biochem.2c00492
Biochemistry 2022, 61, 2897−2908

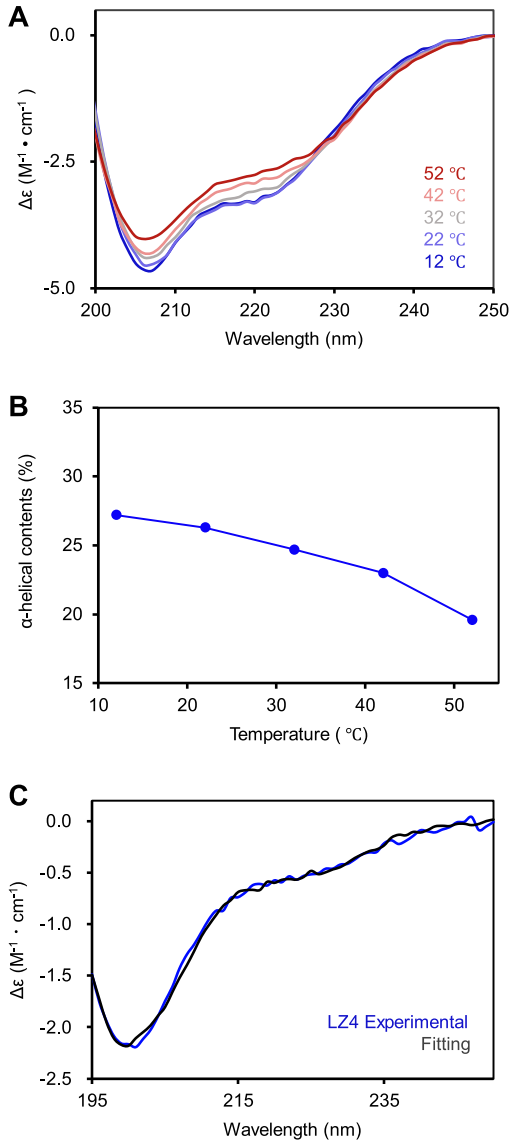

Figure 6. Temperature-dependent secondary structural change. (A) CD spectra of Hsf1 at varying temperatures from 12 to 52 °C. (B) α-Helical contents (%) calculated using BeStSel dependence on temperature change. (C) CD spectra of Hsf1 LZ4 at 12 °C.

with the blue-native gel electrophoresis results in the previous study.[22] Therefore, CD measurements showed that the intermediate state in the transition from the monomer to the oligomer at elevated temperature is coupled with the helical unfolding.

DISCUSSION

Hsf1 oligomerization is a key event during stress response; however, insight into how Hsf1 transitions from monomer to oligomer is limited because of the lack of studies that have monitored the three-dimensional conformational changes of Hsf1. In this study, we aimed to elucidate the mechanism of the heat-induced conformational transition and oligomerization of Hsf1. Trp fluorescence measurements revealed that Hsf1 oligomerizes through an intermediate (Figures 1D,E and 4A,B), and its model fitting, ANS fluorescence measurements, and SEC−MALS revealed that the intermediate is a monomeric open conformation in which the interaction between LZ1−3 and LZ4 was resolved (Figures 1C−E, 2, 3, 5A,B and S3). Furthermore, the CD experiments showed that the weakening of the interaction between LZ1−3 and LZ4 was coupled with the unfolding of the helical structure (Figures 6, S6, and S7). Especially, LZ4 was found to be prone to unfolding (Figure 6C). These data are consistent with the previous study using hydrogen/deuterium-exchange mass spectrometry, showing destabilization of LZ4 at elevated temperatures.[22] Therefore, the data suggest that heat-induced unfolding of LZ4 occurs in conjunction with the tertiary structural change from the closed to open conformation of Hsf1 (Figure S8).

Trp and ANS fluorescence at different temperatures showed that Hsf1 exists in an open conformational intermediate at the temperature range between 30 and 40 °C (Figures 3 and 5). Although intracellular crowding environment and other regulatory factors may have an influence,[52] the monomeric open conformation may be the major conformation at normal cell temperature.[53] Such an open conformation of the Hsf1 monomer, which exposes the sites involved in oligomerization, may allow the rapid formation of the active oligomer under stress. Hsf1 is known to form a complex with several molecular chaperones,[14−17] and the proposed sites for interaction with Hsp70, Hsp90, and TRiC are located in regions LZ1−3 and RegD.[14,17,54] Moreover, it is also suggested that the nuclear localization signal, which is recognized by nuclear transporters, is located immediately after LZ1-3 (residues: 203−230).[18] The locations of chaperone-binding sites and nuclear localization signals around LZ1-3 imply the importance of the open-close conformational change of Hsf1 mediated by the contact between LZ1−3 and LZ4 for the regulation of interaction with other molecules (Figure S8). Interestingly, the previous cell-based study showed that Hsf1 mutant disrupting the interaction between LZ1−3 and LZ4 accumulates in the nucleus,[33] highlighting the possible relationship between Hsf1 open-close conformational state and recognition by the regulators. Thus, the conformational regulation of Hsf1 by molecular chaperones, in addition to the intramolecular LZ interactions to maintain the open monomeric state as the major fraction, can be advantageous in stress responses such as oligomerization and nuclear transport when cells are under stress. Our findings show that Hsf1 oligomerizes through a monomeric open intermediate. Furthermore, this monomeric open state is not just an intermediate in oligomerization but can be a major conformational state in the intracellular environment and a key to understanding the regulation of Hsf1-mediated stress response through interactions with multiple cellular components.

CONCLUSIONS

The oligomerization of Hsf1 is considered as an important step in HSR; however, the lack of information about structural change via oligomerization at heat response impeded the understanding of the thermosensing mechanism through oligomerization. In this study, we applied solution biophysical methods and showed that Hsf1 undergoes monomer-to-oligomer change through the intermediate open state in which the intramolecular LZ interaction is dissolved, as the temperature increases. This conformational change is coupled with the unfolding of LZ helices. Such an open conformation of the Hsf1 monomer, which exposes the sites involved in oligomerization, may allow the rapid formation of the active oligomer under stress. Moreover, since the interaction sites

https://doi.org/10.1021/acs.biochem.2c00492
Biochemistry 2022, 61, 2897−2908

with molecular chaperones and nuclear transporters are also expected to be exposed in the open conformation, the conformational change to the open state can be a key to understanding the regulation of Hsf1-mediated stress response through interaction with multiple cellular components.

■ ASSOCIATED CONTENT

Supporting Information

The Supporting Information is available free of charge at https://pubs.acs.org/doi/10.1021/acs.biochem.2c00492.

GB1 fluorescence spectra, hydrophobic cavity of Hsf1 monomer/trimer, SEC−MALS results of Hsf1, SVD analysis of the fluorescence spectral data, ANS fluorescence with DBD, experimental CD spectra, its curve fitting, MD simulation of LZ4, and proposed model of the Hsf1 open/close conformational change (PDF)

■ AUTHOR INFORMATION

Corresponding Authors

Koichiro Ishimori − *Graduate School of Chemical Sciences and Engineering, Hokkaido University, Sapporo, Hokkaido 060-8628, Japan; Department of Chemistry, Faculty of Science, Hokkaido University, Sapporo, Hokkaido 060-0810, Japan;* orcid.org/0000-0002-5868-0462; Phone: +81-11-706-2707; Email: koichiro@sci.hokudai.ac.jp; Fax: +81-11-706-3501

Tomohide Saio − *Graduate School of Medical Sciences, Institute of Advanced Medical Sciences, and Fujii Memorial Institute of Medical Sciences, Institute of Advanced Medical Sciences, Tokushima University, Tokushima 770-8503, Japan;* orcid.org/0000-0003-3639-7399; Phone: +81-88-633-9149; Email: saio@tokushima-u.ac.jp; Fax: +81-88-633-9145

Authors

Soichiro Kawagoe − *Graduate School of Chemical Sciences and Engineering, Hokkaido University, Sapporo, Hokkaido 060-8628, Japan; Graduate School of Medical Sciences, Tokushima University, Tokushima 770-8503, Japan*

Munehiro Kumashiro − *Institute of Advanced Medical Sciences, Tokushima University, Tokushima 770-8503, Japan*

Takuya Mabuchi − *Frontier Research Institute for Interdisciplinary Sciences and Institute of Fluid Science, Tohoku University, Sendai, Miyagi 980-8577, Japan;* orcid.org/0000-0001-8253-4273

Hiroyuki Kumeta − *Faculty of Advanced Life Science, Hokkaido University, Sapporo, Hokkaido 001-0021, Japan*

Complete contact information is available at: https://pubs.acs.org/10.1021/acs.biochem.2c00492

Author Contributions

S.K. and T.S. designed the study. S.K., M.K., T.M., and H.K. conducted the experiments. S.K., M.K., and T.M. analyzed the data. S.K., M.K., T.M., K.I., and T.S. wrote the paper with inputs from all other authors. T.S. conceptualized the study.

Notes

The authors declare no competing financial interest.

■ ACKNOWLEDGMENTS

This work was supported by funding from JSPS KAKENHI (JP20J20761 to S.K.; JP22K20633 to M.K.; JP18H05229, JP20H03199, JP20KK0156, JP21H05093, JP21H05094, JP22K18361, and JP22H02560 to T.S.; and JP19H05769 to K.I.), MEXT Grant-in-Aid for Transformative Research Areas (B) (JP21H05096 to T.M. and JP21H05094 and JP21H05093 to T.S.), AMED (JP21ek0109437 and JP21wm0425004 to T.S.), and JST FOREST Program (JPMJFR212H to T.M.; JPMJFR204W to T.S.). This work was also partially supported by the Takeda Science Foundation Grant, the Kato Memorial Trust for Nambyo Research, the Mochida Memorial Foundation for Medical and Pharmaceutical Research, the Naito Foundation, the Yukihiko Miyata Memorial Trust for ALS Research, and the program of the Inter-University Research Network for High Depth Omics, IAMS, Tokushima University. We also thank Dr. Asuka Mukai (Tokushima University), Dr. Yoshikazu Hattori (Tokushima University), and Ms. Eri Sakamoto (Tokushima University) for their experimental support. The CD and DLS experiments were performed at the Faculty of Pharmaceutical Sciences, Tokushima University. The computational resources for this research were provided in part by the Institute of Fluid Science at Tohoku University. NMR experiments were performed at the Hokkaido University Advanced NMR Facility, a member of the NMR Platform.

■ REFERENCES

(1) Fulda, S.; Gorman, A. M.; Hori, O.; Samali, A. Cellular Stress Responses: Cell Survival and Cell Death. *Int. J. Cell Biol.* **2010**, *2010*, 1.

(2) Jolly, C.; Morimoto, R. I. Role of the Heat Shock Response and Molecular Chaperones in Oncogenesis and Cell Death. *J. Natl. Cancer Inst.* **2000**, *92*, 1564−1572.

(3) Vihervaara, A.; Mahat, D. B.; Guertin, M. J.; Chu, T.; Danko, C. G.; Lis, J. T.; Sistonen, L. Transcriptional Response to Stress Is Pre-Wired by Promoter and Enhancer Architecture. *Nat. Commun.* **2017**, *8*, 1−16.

(4) Mahat, D. B.; Salamanca, H. H.; Duarte, F. M.; Danko, C. G.; Lis, J. T. Mammalian Heat Shock Response and Mechanisms Underlying Its Genome-Wide Transcriptional Regulation. *Mol. Cell* **2016**, *62*, 63−78.

(5) Sarge, K. D.; Murphy, S. P.; Morimoto, R. I. Activation of Heat Shock Gene Transcription by Heat Shock Factor 1 Involves Oligomerization, Acquisition of DNA-Binding Activity, and Nuclear Localization and Can Occur in the Absence of Stress. *Mol. Cell. Biol.* **1993**, *13*, 1392−1407.

(6) Morimoto, R. I. Regulation of the Heat Shock Transcriptional Response: Cross Talk between a Family of Heat Shock Factors, Molecular Chaperones, and Negative Regulators. *Genes Dev.* **1998**, *12*, 3788−3796.

(7) Li, J.; Labbadia, J.; Morimoto, R. I. Rethinking HSF1 in Stress, Development, and Organismal Health. *Trends Cell Biol.* **2017**, *27*, 895−905.

(8) Åkerfelt, M.; Morimoto, R. I.; Sistonen, L. Heat Shock Factors: Integrators of Cell Stress, Development and Lifespan. *Nat. Rev. Mol. Cell Biol.* **2010**, *11*, 545−555.

(9) Trinklein, N. D.; Murray, J. I.; Hartman, S. J.; Botstein, D.; Myers, R. M. The Role of Heat Shock Transcription Factor 1 in the Genome-Wide Regulation of the Mammalian Heat Shock Response. *Mol. Biol. Cell* **2004**, *15*, 1254−1261.

(10) Gonsalves, S. E.; Moses, A. M.; Razak, Z.; Robert, F.; Westwood, J. Whole-Genome Analysis Reveals That Active Heat Shock Factor Binding Sites Are Mostly Associated with Non-Heat Shock Genes in Drosophila Melanogaster. *PLoS One* **2011**, *6*, No. e15934.

(11) Hahn, J.-S.; Hu, Z.; Thiele, D. J.; Iyer, V. R. Genome-Wide Analysis of the Biology of Stress Responses through Heat Shock Transcription Factor. *Mol. Cell. Biol.* **2004**, *24*, 5249−5256.

(12) Jacobs, A. T.; Marnett, L. J. HSF1-Mediated BAG3 Expression Attenuates Apoptosis in 4-Hydroxynonenal-Treated Colon Cancer Cells via Stabilization of Anti-Apoptotic Bcl-2 Proteins. *J. Biol. Chem.* **2009**, *284*, 9176−9183.
(13) Anckar, J.; Sistonen, L. Regulation of HSF1 Function in the Heat Stress Response: Implications in Aging and Disease. *Annu. Rev. Biochem.* **2011**, *80*, 1089−1115.
(14) Kmiecik, S. W.; Le Breton, L.; Mayer, M. P. Feedback Regulation of Heat Shock Factor 1 (Hsf1) Activity by Hsp70-mediated Trimer Unzipping and Dissociation from DNA. *EMBO J.* **2020**, *39*, No. e104096.
(15) Shi, Y.; Mosser, D. D.; Morimoto, R. I. Molecularchaperones as HSF1-specific transcriptional repressors. *Genes Dev.* **1998**, *12*, 654−666.
(16) Zou, J.; Guo, Y.; Guettouche, T.; Smith, D. F.; Voellmy, R. Repression of Heat Shock Transcription Factor HSF1 Activation by HSP90 (HSP90 Complex) That Forms a Stress-Sensitive Complex with HSF1. *Cell* **1998**, *94*, 471−480.
(17) Neef, D. W.; Jaeger, A. M.; Gomez-Pastor, R.; Willmund, F.; Frydman, J.; Thiele, D. J. A Direct Regulatory Interaction between Chaperonin TRiC and Stress-Responsive Transcription Factor HSF1. *Cell Rep.* **2014**, *9*, 955−966.
(18) Vujanac, M.; Fenaroli, A.; Zimarino, V. Constitutive Nuclear Import and Stress-Regulated Nucleocytoplasmic Shuttling of Mammalian Heat-Shock Factor 1. *Traffic* **2005**, *6*, 214−229.
(19) Goodson, M. L.; Sarge, K. D. Heat-Inducible DNA Binding of Purified Heat Shock Transcription Factor 1. *J. Biol. Chem.* **1995**, *270*, 2447−2450.
(20) Sarge, K. D.; Murphy, S. P.; Morimoto, R. I. Activation of Heat Shock Gene Transcription by Heat Shock Factor 1 Involves Oligomerization, Acquisition of DNA-Binding Activity, and Nuclear Localization and Can Occur in the Absence of Stress. *Mol. Cell. Biol.* **1993**, *13*, 1392−1407.
(21) Rabindran, S. K.; Haroun, R. I.; Clos, J.; Wisniewski, J.; Wu, C. Regulation of Heat Shock Factor Trimer Formation: Role of a Conserved Leucine Zipper. *Science* **1993**, *259*, 230−234.
(22) Hentze, N.; Le Breton, L.; Wiesner, J.; Kempf, G.; Mayer, M. P. Molecular Mechanism of Thermosensory Function of Human Heat Shock Transcription Factor Hsf1. *Elife* **2016**, *5*, No. e11576.
(23) Zhong, M.; Orosz, A.; Wu, C. Direct Sensing of Heat and Oxidation by Drosophila Heat Shock Transcription Factor. *Mol. Cell* **1998**, *2*, 101−108.
(24) Zuo, J.; Baler, R.; Dahl, G.; Voellmy, R. Activation of the DNA-Binding Ability of Human Heat Shock Transcription Factor 1 May Involve the Transition from an Intramolecular to an Intermolecular Triple-Stranded Coiled-Coil Structure. *Mol. Cell. Biol.* **1994**, *14*, 7557−7568.
(25) Westwood, J. T.; Wu, C. Activation of Drosophila Heat Shock Factor: Conformational Change Associated with a Monomer-to-Trimer Transition. *Mol. Cell. Biol.* **1993**, *13*, 3481−3486.
(26) Dai, C. The Heat-Shock, or HSF1-Mediated Proteotoxic Stress, Response in Cancer: From Proteomic Stability to Oncogenesis. *Philos. Trans. R. Soc., B* **2018**, *373*, 20160525.
(27) Mendillo, M. L.; Santagata, S.; Koeva, M.; Bell, G. W.; Hu, R.; Tamimi, R. M.; Fraenkel, E.; Ince, T. A.; Whitesell, L.; Lindquist, S. HSF1 Drives a Transcriptional Program Distinct from Heat Shock to Support Highly Malignant Human Cancers. *Cell* **2012**, *150*, 549−562.
(28) Gomez-Pastor, R.; Burchfiel, E. T.; Neef, D. W.; Jaeger, A. M.; Cabiscol, E.; McKinstry, S. U.; Doss, A.; Aballay, A.; Lo, D. C.; Akimov, S. S.; Ross, C. A.; Eroglu, C.; Thiele, D. J. Abnormal Degradation of the Neuronal Stress-Protective Transcription Factor HSF1 in Huntington's Disease. *Nat. Commun.* **2017**, *8*, 1−17.
(29) Neudegger, T.; Verghese, J.; Hayer-Hartl, M.; Hartl, F. U.; Bracher, A. Structure of Human Heat-Shock Transcription Factor 1 in Complex with DNA. *Nat. Struct. Mol. Biol.* **2016**, *23*, 140−146.
(30) Feng, N.; Feng, H.; Wang, S.; Punekar, A. S.; Ladenstein, R.; Wang, D. C.; Zhang, Q.; Ding, J.; Liu, W. Structures of Heat Shock Factor Trimers Bound to DNA. *iScience* **2021**, *24*, 102951.
(31) Nelson, O.; Littlefield, H. C. M. A New Use for the "wing" of the "Winged" Helix-Turn-Helix Motif in the HSF−DNA Cocrystal. *Nat. Struct. Biol.* **1999**, *6*, 464−470.
(32) Jaeger, A. M.; Makley, L. N.; Gestwicki, J. E.; Thiele, D. J. Genomic Heat Shock Element Sequences Drive Cooperative Human Heat Shock Factor 1 DNA Binding and Selectivity. *J. Biol. Chem.* **2014**, *289*, 30459−30469.
(33) Neef, D. W.; Jaeger, A. M.; Thiele, D. J. Genetic Selection for Constitutively Trimerized Human Hsf1 Mutants Identifies a Role for Coiled-Coil Motifs in DNA Binding. *G3: Genes, Genomes, Genet.* **2013**, *3*, 1315−1324.
(34) Shashilov, V. A.; Lednev, I. K. Advanced Statistical and Numerical Methods for Spectroscopic Characterization of Protein Structural Evolution. *Chem. Rev.* **2010**, *110*, 5692−5713.
(35) Micsonai, A.; Wien, F.; Kernya, L.; Lee, Y. H.; Goto, Y.; Réfrégiers, M.; Kardos, J. Accurate Secondary Structure Prediction and Fold Recognition for Circular Dichroism Spectroscopy. *Proc. Natl. Acad. Sci. U.S.A.* **2015**, *112*, E3095−E3103.
(36) Huang, J.; Rauscher, S.; Nawrocki, G.; Ran, T.; Feig, M.; de Groot, B. L.; Grubmüller, H.; MacKerell, A. D. CHARMM36m: An Improved Force Field for Folded and Intrinsically Disordered Proteins. *Nat. Methods* **2016**, *14*, 71−73.
(37) Plimpton, S. Fast Parallel Algorithms for Short-Range Molecular Dynamics. *J. Comput. Phys.* **1995**, *117*, 1−19.
(38) Jumper, J.; Evans, R.; Pritzel, A.; Green, T.; Figurnov, M.; Ronneberger, O.; Tunyasuvunakool, K.; Bates, R.; Žídek, A.; Potapenko, A.; Bridgland, A.; Meyer, C.; Kohl, S. A. A.; Ballard, A. J.; Cowie, A.; Romera-Paredes, B.; Nikolov, S.; Jain, R.; Adler, J.; Back, T.; Petersen, S.; Reiman, D.; Clancy, E.; Zielinski, M.; Steinegger, M.; Pacholska, M.; Berghammer, T.; Bodenstein, S.; Silver, D.; Vinyals, O.; Senior, A. W.; Kavukcuoglu, K.; Kohli, P.; Hassabis, D. Highly Accurate Protein Structure Prediction with AlphaFold. *Nature* **2021**, *596*, 583−589.
(39) Nosé, S. A Molecular Dynamics Method for Simulations in the Canonical Ensemble. *Mol. Phys.* **2006**, *52*, 255−268.
(40) Hoover, W. G. Constant-Pressure Equations of Motion. *Phys. Rev. A* **1986**, *34*, 2499.
(41) Martyna, G. J.; Tobias, D. J.; Klein, M. L. Constant Pressure Molecular Dynamics Algorithms. *J. Chem. Phys.* **1994**, *101*, 4177.
(42) Parrinello, M.; Rahman, A. Polymorphic Transitions in Single Crystals: A New Molecular Dynamics Method. *J. Appl. Phys.* **1981**, *52*, 7182.
(43) Hockney, R. W.; Eastwood, J. W. *Computer Simulation Using Particles*; crc Press, 1989.
(44) Verlet, L. Computer "Experiments" on Classical Fluids. I. Thermodynamical Properties of Lennard-Jones Molecules. *Phys. Rev.* **1967**, *159*, 98.
(45) Ryckaert, J.-P.; Ciccotti, G.; Berendsen, H. J. C. Numerical Integration of the Cartesian Equations of Motion of a System with Constraints: Molecular Dynamics of n-Alkanes. *J. Comput. Phys.* **1977**, *23*, 327−341.
(46) Kabsch, W.; Sander, C. Dictionary of Protein Secondary Structure: Pattern Recognition of Hydrogen-Bonded and Geometrical Features. *Biopolymers* **1983**, *22*, 2577−2637.
(47) Gronenborn, A. M.; Filpula, D. R.; Essig, N. Z.; Achari, A.; Whitlow, M.; Wingfield, P. T.; Clore, G. M. A Novel, Highly Stable Fold of the Immunoglobulin Binding Domain of Streptococcal Protein G. *Science* **1991**, *253*, 657−661.
(48) Vivian, J. T.; Callis, P. R. Mechanisms of Tryptophan Fluorescence Shifts in Proteins. *Biophys. J.* **2001**, *80*, 2093−2109.
(49) Mól, A. R.; Castro, M. S.; Fontes, W. NetWheels: A Web Application to Create High Quality Peptide Helical Wheel and Net Projections. *bioRxiv* **2018**, 416347.
(50) Gasymov, O. K.; Glasgow, B. J. ANS Fluorescence: Potential to Augment the Identification of the External Binding Sites of Proteins. *Biochim. Biophys. Acta, Proteins Proteomics* **2007**, *1774*, 403−411.
(51) Latypov, R. F.; Liu, D.; Gunasekaran, K.; Harvey, T. S.; Razinkov, V. I.; Raibekas, A. A. Structural and Thermodynamic

https://doi.org/10.1021/acs.biochem.2c00492
Biochemistry 2022, 61, 2897−2908

Effects of ANS Binding to Human Interleukin-1 Receptor Antagonist. *Protein Sci.* **2008**, *17*, 652−663.
(52) Okabe, K.; Inada, N.; Gota, C.; Harada, Y.; Funatsu, T.; Uchiyama, S. Intracellular Temperature Mapping with a Fluorescent Polymeric Thermometer and Fluorescence Lifetime Imaging Microscopy. *Nat. Commun.* **2012**, *3*, 1−9.
(53) Ellis, R. J. Macromolecular Crowding: Obvious but Underappreciated. *Trends Biochem. Sci.* **2001**, *26*, 597−604.
(54) Kijima, T.; Prince, T. L.; Tigue, M. L.; Yim, K. H.; Schwartz, H.; Beebe, K.; Lee, S.; Budzynski, M. A.; Williams, H.; Trepel, J. B.; Sistonen, L.; Calderwood, S.; Neckers, L. HSP90 Inhibitors Disrupt a Transient HSP90-HSF1 Interaction and Identify a Noncanonical Model of HSP90-Mediated HSF1 Regulation. *Sci. Rep.* **2018**, *8*, 1−13.

https://doi.org/10.1021/acs.biochem.2c00492
Biochemistry 2022, 61, 2897−2908